Mixed-hybrid finite element method for modelling two-phase flow in porous media

Fučík, Radek
Department of Mathematics, Faculty of Nuclear Sciences and Physical Engineering, Czech Technical University

Mikyška, Jiří
Department of Mathematics, Faculty of Nuclear Sciences and Physical Engineering, Czech Technical University

出版情報：Journal of Math-for-Industry (JMI). 3 (C), pp.9-19, 2012-01-27. Faculty of Mathematics, Kyushu University
バージョン：
権利関係：

Journal of Math-for-Industry, Vol. 3 (2011C-2), pp. 9–19

Math-for-industry
Education & Research Hub

Mixed-hybrid finite element method for modelling two-phase flow in porous media

Radek Fučík and Jiří Mikyška

Revised on September 23, 2011

Abstract. We propose a new numerical scheme for simulation of flow of two immiscible and incompressible phases in porous media. The method is based on a combination of the mixed-hybrid finite element (MHFE) and discontinuous Galerkin (DG) methods. The combined approach allows for accurate approximation of the flux at the boundary between neighboring finite elements, especially in heterogeneous media. We extend the method proposed in [12] to simulate the non-wetting phase pooling at material interfaces. In order to show its applicability, the MHFE-DG method is tested against benchmark solutions and using laboratory data from literature.

Keywords. MHFE-DG method, Two-phase flow, Heterogeneous porous media

1. Introduction

Most of the industrially developed countries invest substantial amounts of resources to understand and protect drinking water in the subsurface. Due to industrial activities, the water saturated aquifers are endangered by substances with a very low solubility in water such as oil or chlorinated hydrocarbons. When these substances, generally referred to as Non-Aqueous Phase Liquids (NAPLs), enter the aquifer, they can serve as a long-time source of groundwater contamination. A prediction of their behavior in the subsurface is an important step towards their partial or complete removal from the contaminated area. Therefore, two-phase processes have been studied intensively in engineering, soil physics, and hydrogeology over several decades [1], [9]. The propagation of NAPLs through water saturated zones is usually driven by two primary mechanisms. The NAPL is displaced due to external forces (externally imposed flow, gravity) and capillarity. Especially in a heterogeneous porous media, the capillary forces have an important impact on the flow across interfaces between materials with different capillarity properties, [14].

In order to model two-phase flow in heterogeneous porous materials, a large number of numerical methods has been developed based on the finite difference (FD), finite volume (FV), or finite element (FE) methods. These methods have typically low accuracy. The FD method is applicable only for orthogonal meshes and the conventional FV method is strongly influenced by the mesh quality and orientation, which makes these methods unsuitable for a large number of real world problems modelled using unstructured grids [17]. There have been attempts to improve accuracy of the FV approach on unstructured meshes by using multi-point flux approximation techniques. However, such techniques have not been demonstrated to be of value for heterogeneous media [13]. Another effort to develop a higher–order numerical scheme was based on the mixed-hybrid finite element (MHFE) method such as [15]. However, none of the proposed MHFE formulations were able to simulate two-phase flow in heterogeneous porous media with discontinuities in saturations at material interfaces that are caused by different capillary pressure functions. Recently, Hoteit and Firoozabadi [11], [12], [13], developed a higher–order numerical method that combines the MHFE approach and the discontinuous Galerkin (DG) method, together denoted as MHFE-DG. Their approach can be used to model two–phase flow in a heterogeneous porous medium with sharp jumps in saturation across material interfaces. We build upon their ideas and extend their approach so that the scheme can simulate the non-wetting phase pooling at material heterogeneity. The use of MHFE-DG allows for accurate representation of the phase velocities across sides of finite elements and approximates saturation as piecewise discontinuous per elements. This facilitates discretization of the two-phase flow problems especially in case of heterogeneous porous materials and fractured media, where the saturation is often discontinuous across sharp heterogeneity interfaces.

The paper is organized in the following way. First, the governing equations are summarized and the problem formulation is derived. Then, the MHFE-DG discretization is described and numerical experiments are presented to demonstrate its applicability.

2. Model Equations

The mathematical model of multi-phase flow in porous media is based on the assumption that every fluid phase is governed by the continuity theorem and the Darcy law. In

the following, we consider a wetting phase (e.g., water) and a non-wetting phase (e.g., air or oil) indexed by w and n, respectively. The α-phase mass balance for $\alpha \in \{w, n\}$ has the following form

$$\frac{\partial(\phi \varrho_\alpha S_\alpha)}{\partial t} + \nabla\cdot(\varrho_\alpha \, \mathbf{u}_\alpha) = \varrho_\alpha F_\alpha, \tag{1}$$

and the Darcy law for the phase α reads as

$$\mathbf{u}_\alpha = -\frac{k_{r,\alpha}}{\mu_\alpha}\mathbf{K}(\nabla p_\alpha - \varrho_\alpha \, \mathbf{g}), \tag{2}$$

where ϕ $[-]$ is the porosity of the medium, $\mathbf{K}$ $[m^2]$ is the intrinsic permeability tensor, and $\mathbf{g}$ $[m\ s^{-2}]$ is the gravitational acceleration vector. For $\alpha \in \{w, n\}$, the symbols ϱ_α, S_α, $\mathbf{u}_\alpha$, F_α, μ_α, $k_{r,\alpha}$, and p_α stand for the α-phase density $[kg\ m^{-3}]$, saturation $[-]$, apparent macroscopic velocity $[m\ s^{-1}]$, specific source/sink term $[s^{-1}]$, dynamic viscosity $[kg\ m^{-1}\ s^{-1}]$, relative permeability $[-]$, and pressure $[kg\ m^{-1}\ s^{-2}]$, respectively. By definition, $S_w + S_n = 1$. We use the Burdine model for the relative permeability functions [4]

$$k_{r,w}(S_{we}) = S_{we}^{3+\frac{2}{\lambda}}, \tag{3}$$

$$k_{r,n}(S_{we}) = (1 - S_{we})^2(1 - S_{we}^{1+\frac{2}{\lambda}}), \tag{4}$$

where the parameter λ $[-]$ is determined experimentally and S_{we} is the effective wetting-phase saturation defined as $S_{we} = (S_w - S_{wr})/(1 - S_{wr})$, where S_{wr} is the irreducible wetting-phase saturation. The term $k_{r,\alpha}/\mu_\alpha$, frequently denoted as the α-phase *mobility* λ_α, allows to rewrite the Darcy law as

$$\mathbf{u}_\alpha = -\lambda_\alpha \mathbf{K}(\nabla p_\alpha - \varrho_\alpha \, \mathbf{g}). \tag{5}$$

In order to close the system of equations, one more equation is added to the system that models the effects of the capillary forces. By definition, the capillary pressure is the difference between the non-wetting and the wetting phase pressures

$$p_c = p_n - p_w \tag{6}$$

and is considered to be a function of saturation S_w. A commonly acknowledged model for $p_c = p_c(S_w)$ is the Brooks and Corey model [3]

$$p_c(S_{we}) = p_d S_{we}^{-\frac{1}{\lambda}} \quad \text{for} \quad S_{we} \in (0, 1], \tag{7}$$

where λ is the same parameter as in (2) and p_d $[Pa]$ is the *entry pressure*. The entry pressure p_d is the capillary pressure at full saturation which is the minimal capillary pressure required to displace the wetting phase from the largest occurring pore.

Let us consider an initially fully water saturated column with two sands separated by a sharp interface. Since no mass is lost or produced at the material interface, the mass conservation law states that the normal component of the *mass flux*

$$\varrho_\alpha \, \mathbf{u}_\alpha \cdot \mathbf{n} \text{ is continuous across the interface,} \tag{8}$$

where $\mathbf{n}$ denotes a unit normal to the interface (see Figure 1). Assuming that a mobile wetting phase is present on both sides of the interface, it follows that (c.f. [16])

$$p_w \text{ is continuous across the interface.} \tag{9}$$

If a non-wetting phase is present on both sides of the interface, p_n is also assumed to be continuous which implies the continuity of the capillary pressure p_c in that case. On the other hand, if the non-wetting phase is not present but approaches the material interface from the coarse sand side, the following situation can occur. If the non-wetting phase reaches the material interface from the coarse sand (denoted by the superscript I), the interfacial capillary pressure p_c^I increases. When p_c^I is lower than the entry pressure p_d^{II} of the finer medium, the non-wetting phase cannot penetrate the interface and accumulates (pools) at the interface. In this case both p_c and p_n are discontinuous. This is referred to as the *barrier effect* [16]. Once the capillary pressure p_c^I exceeds the entry pressure threshold p_d^{II}, the non-wetting phase enters the finer sand and the capillary pressure p_c is continuous, i.e., $p_c^I = p_c^{II}$, while the saturation can be discontinous. In Figure 2, typical Brooks and Corey capillary pressure curves (7) for two different porous media are shown. Altogether, the condition at the material interface is established in the following form:

$$\begin{array}{ll} S_n^{II} = 0 \quad \text{and} \quad p_c^{II} = p_d^{II}, & \text{if} \quad p_c^I < p_d^{II}, \\ p_c^I = p_c^{II}, & \text{otherwise.} \end{array} \tag{10}$$

Eq. (10) is referred to as the *extended capillary pressure condition* [16]. A unique value of the wetting phase saturation $S_w^{I,*}$ can be associated with the threshold value of the capillary pressure such that

$$S_w^{I,*} = (p_c^I)^{-1}(p_d^{II}), \tag{11}$$

see Figure 2. The threshold saturation $S_w^{I,*}$ indicates whether the non-wetting phase can penetrate the material interface ($S_w^I \le S_w^{I,*}$) or the barrier effect is simulated ($S_w^I > S_w^{I,*}$).

3. Problem Formulation

Since we assume that both fluids are incompressible, we introduce the *flow potential* ψ_α as

$$\psi_\alpha = p_\alpha - \varrho_\alpha \, \mathbf{g}\cdot\mathbf{x}, \tag{12}$$

where $\mathbf{x}$ is the position vector and $\alpha \in \{w, n\}$. Similarly to the definition of the capillary pressure (6), we define the *capillary potential* as

$$\psi_c = \psi_n - \psi_w = p_c - (\rho_n - \rho_w)\mathbf{g}\cdot\mathbf{x}. \tag{13}$$

Consequently, the system of equations can be rewritten in the following form

$$\phi\frac{\partial S_\alpha}{\partial t} + \nabla\cdot\mathbf{u}_\alpha = F_\alpha, \tag{14a}$$

$$\mathbf{u}_\alpha = -\lambda_\alpha \mathbf{K}\nabla\psi_\alpha, \tag{14b}$$

$$\psi_c = \psi_n - \psi_w, \tag{14c}$$

$$S_w + S_n = 1, \tag{14d}$$

where $\alpha \in \{w, n\}$ and the unknown functions are the saturations $S_\alpha = S_\alpha(t, \mathbf{x})$ and the phase potentials $\psi_\alpha = \psi_\alpha(t, \mathbf{x})$ for all $t > 0$ and $\mathbf{x}$ inside a domain $\Omega \subset \mathbb{R}^d$, $d = 1, 2, 3$. Equations (14) are subject to an initial condition

$$S_\alpha = S_\alpha^{ini}, \quad \text{in} \quad \Omega, \tag{15}$$

and boundary conditions

$$\mathbf{u}_\alpha \cdot \mathbf{n} = u_\alpha^{\mathcal{N}} \quad \text{on} \quad \Gamma_{\mathbf{u}_\alpha} \subset \partial\Omega, \tag{16a}$$

$$S_w = S_w^{\mathcal{D}} \quad \text{on} \quad \Gamma_{S_w} \subset \partial\Omega, \tag{16b}$$

$$\psi_\alpha = \psi_\alpha^{\mathcal{D}} \quad \text{on} \quad \Gamma_{\psi_\alpha} \subset \partial\Omega, \tag{16c}$$

where $\Gamma_{\mathbf{u}_\alpha}$, Γ_{S_w}, and Γ_{ψ_α} denote the subsets of the domain boundary $\partial\Omega$ where the boundary conditions for $\mathbf{u}_\alpha$, S_w, and ψ_α are prescribed, respectively, $\alpha \in \{w, n\}$. The superscripts $\mathcal{N}$ and $\mathcal{D}$ stand for the Neumann and Dirichlet type boundary conditions, respectively. The initial condition (15) and boundary conditions (16) should be consistent with (14c) and (14d).

Summing (14a) over $\alpha = \{w, n\}$ and using (14d), we obtain the following equation for the divergence of the *total velocity* $\mathbf{u}_t = \mathbf{u}_w + \mathbf{u}_n$,

$$\nabla\cdot\mathbf{u}_t = \nabla\cdot(\mathbf{u}_w + \mathbf{u}_n) = F_w + F_n \quad \text{in} \quad \Omega. \tag{17}$$

We define new velocities $\mathbf{u}_a$ and $\mathbf{u}_c$

$$\mathbf{u}_a = -\lambda_t \mathbf{K}\nabla\psi_w, \qquad \mathbf{u}_c = -\lambda_t \mathbf{K}\nabla\psi_c, \tag{18}$$

where the velocity $\mathbf{u}_a$ has the same driving force as the velocity $\mathbf{u}_w$ but with a smoother total mobility $\lambda_t = \lambda_w + \lambda_n$ and the velocity $\mathbf{u}_c$ includes the capillary driving forces. Hence, the total velocity $\mathbf{u}_t$ reads as

$$\mathbf{u}_t = \mathbf{u}_a + f_n \mathbf{u}_c, \tag{19}$$

where $f_n = \lambda_n/\lambda_t$ is the fractional flow function of the non-wetting phase. In contrast to [13] where the capillary velocity $\mathbf{u}_c$ is defined as

$$\mathbf{u}_c^{HF} = -\lambda_n \mathbf{K}\nabla\psi_c, \tag{20}$$

we use the definition (18) since we will need to invert $\lambda_t\mathbf{K}$ in the relationship (18) in order to obtain an explicit expression for $\nabla\psi_c$. This is always possible since $\lambda_t = \lambda_t(S_w)$ is strictly positive for all S_w. However, a similar inversion cannot be done using the definition (20) since the non-wetting phase mobility λ_n vanishes as $S_w \to 1$.

The phase velocities $\mathbf{u}_w$ and $\mathbf{u}_n$, can be expressed in terms of $\mathbf{u}_a$ and $\mathbf{u}_c$ as

$$\mathbf{u}_w = f_w \mathbf{u}_a, \qquad \mathbf{u}_n = f_n \mathbf{u}_a + f_n \mathbf{u}_c, \tag{21}$$

where $f_w = \lambda_w/\lambda_t$ is the fractional flow function of the wetting phase. In order to express the velocities $\mathbf{u}_a$ and $\mathbf{u}_c$ in terms of the phase velocities $\mathbf{u}_w$ and $\mathbf{u}_n$, we consider the inverse relationship:

$$\mathbf{u}_a = \begin{cases} 0 & \text{if} \quad f_w = 0, \\ f_w^{-1}\mathbf{u}_w & \text{otherwise}, \end{cases} \tag{22a}$$

$$\mathbf{u}_c = \begin{cases} -\mathbf{u}_w & \text{if} \quad f_n = 0, \\ \mathbf{u}_n & \text{if} \quad f_w = 0, \\ f_n^{-1}\mathbf{u}_n - f_w^{-1}\mathbf{u}_w & \text{otherwise}, \end{cases} \tag{22b}$$

where we assume that the value of the fractional flow functions are nonzero ($f_\alpha \neq 0$), if $\mathbf{u}_\alpha \neq 0$, $\alpha \in \{w, n\}$. This assumption is consistent with the definition of the phase mobility, i.e., the α-phase mobility cannot be zero if the phase velocity is nonzero. The evolution equation for the wetting phase saturation (14a) in terms of $\mathbf{u}_a$ reads as

$$\phi\frac{\partial S_w}{\partial t} + \nabla\cdot(f_w\mathbf{u}_a) = F_w. \tag{23}$$

4. Discretization

We consider a spatial discretization $\mathcal{K}_h$ of the polygonal domain Ω consisting of elements K, where K are segments in $\mathbb{R}$ or triangles in $\mathbb{R}^2$ and $h > 0$ is the *mesh size* defined as the maximum element diameter. We assume that the mesh is regular and conforming, i.e., the intersection of two elements is either empty, a vertex, or an edge. We denote by $\mathcal{V}_h$ the set of all vertices V of $\mathcal{K}_h$, by $\mathcal{E}_h$ the set of all sides of $\mathcal{K}_h$, and by $\mathcal{E}_h^{int}$ and $\mathcal{E}_h^{ext}$ the set of interior and exterior sides of $\mathcal{K}_h$, respectively. By $\mathcal{E}_K$, we denote the set of all sides of an element $K \in \mathcal{K}_h$.

4.1. Velocity Approximation

We assume, that the velocities $\mathbf{u}_\alpha$, where $\alpha \in \{w, n, a, c\}$, belong to the functional space $\mathbf{H}(\mathrm{div}, \Omega) = \{\mathbf{v} \in [L^2(\Omega)]^d; \nabla\cdot\mathbf{v} \in L^2(\Omega)\}$, which is the space of functions with square–integrable weak divergences. On each element $K \in \mathcal{K}_h$, we shall approximate the phase velocities $\mathbf{u}_\alpha$ in the lowest order Raviart–Thomas space $\mathbf{RT}_0(K)$. The space $\mathbf{RT}_0(\mathcal{K}_h) \subset \mathbf{H}(\mathrm{div}, \Omega)$ is a space of vector functions that are piecewise linear per elements $K \in \mathcal{K}_h$. The basis functions $\mathbf{w}_{K,E} \in \mathbf{RT}_0(K)$ are chosen such that

$$\mathbf{w}_{K,E}\cdot\mathbf{n}_{K,F} = \delta_{EF}\frac{1}{|E|_{\text{d-1}}}, \qquad \forall E, F \in \mathcal{E}_K, \tag{24a}$$

$$\nabla\cdot\mathbf{w}_{K,E} = \frac{1}{|K|_{\text{d}}}, \qquad \forall E \in \mathcal{E}_K, \tag{24b}$$

where $\mathbf{n}_{K,E}$ is the outward unit normal to side $E \in \mathcal{E}_K$ with respect to element K, d denotes the dimension of $\mathbb{R}^d$, δ_{EF} is the Kronecker symbol, and $|\cdot|_{\text{d}}$ is a d-dimensional Lebesque measure. Note that for convenience, we set $|E|_0 = 1$ for all $E \in \mathcal{E}_K$.

The velocity $\mathbf{u}_\alpha$ is approximated in the basis of $\mathbf{RT}_0(K)$, $K \in \mathcal{K}_h$ as

$$\mathbf{u}_\alpha = \sum_{E\in\mathcal{E}_K} u_{\alpha,K,E}\mathbf{w}_{K,E}, \quad \alpha \in \{a, c\}, \tag{25}$$

where $u_{\alpha,K,E}$ are the side–flux variables across the side $E \in \mathcal{E}_K$ in the outward direction with respect to K.

By inverting the permeability tensor $\mathbf{K}$ and the total mobility λ_t in (18), we obtain

$$\lambda_t^{-1}\mathbf{K}^{-1}\mathbf{u}_a = -\nabla\psi_w, \tag{26}$$

where we assume that $\mathbf{K}$ is positive definite and $\lambda_t = \lambda_t(S_w)$ strictly positive for all S_w. The variational formulation is obtained by multiplying (26) by the test functions from $\mathbf{RT}_0(\mathcal{K}_h)$ that are represented on each element $K \in \mathcal{K}_h$ by the $\mathbf{RT}_0(K)$ basis functions $\mathbf{w}_{K,E}$. We integrate the resulting product by parts over K and using the properties of the $\mathbf{RT}_0(K)$ basis functions (24) we obtain from the left–hand–side of (26):

$$\int_K \lambda_t^{-1}\mathbf{w}_{K,E}\mathbf{K}^{-1}\mathbf{u}_a = \lambda_{t,K}^{-1}\sum_{F\in\mathcal{E}_K} u_{a,K,F}A_{K,E,F} \qquad (27)$$

and from the right–hand–side of (26):

$$-\int_K \nabla\psi_w\cdot\mathbf{w}_{K,E} = -\int_{\partial K}\psi_w\mathbf{w}_{K,E}\cdot\mathbf{n}_{\partial K} - \int_K \psi_w\nabla\cdot\mathbf{w}_{K,E} = \\ = \frac{1}{|K|_{\mathrm{d}}}\int_K \psi_w - \frac{1}{|E|_{\mathrm{d-1}}}\int_E \psi_w = \psi_{w,K} - \psi_{w,E}, \qquad (28)$$

where $\lambda_{t,K}$ is the average of λ_t over K and by $\psi_{w,K}$ and $\psi_{w,F}$ we denote the cell- and side-averages of the potential ψ_w, respectively. The coefficients $\{A_{K,E,F}\}_{E,F\in\mathcal{E}_K}$ in (27) are given by

$$A_{K,E,F} = \int_K \mathbf{w}_{K,E}\mathbf{K}^{-1}\mathbf{w}_{K,F}, \qquad (29)$$

and form a local matrix $\mathbf{A}_K$ on K. Under the assumption that $\mathbf{K}$ is a symmetric and positive definite tensor, $\mathbf{A}_K$ is symmetric, positive definite, and therefore invertible. By $\mathbf{a}_K = \{a_{K,E,F}\}_{E,F\in\mathcal{E}_K}$, we denote the inversion of $\mathbf{A}_K$, i.e., $\mathbf{a}_K = \mathbf{A}_K^{-1}$. The coefficients $a_{K,E,F}$ depend only on the mesh $\mathcal{K}_h$ and the value of the intrinsic permeability tensor $\mathbf{K}$. Using this notation, the side–fluxes $u_{a,K,E}$ satisfy

$$u_{a,K,E} = \lambda_{t,K}\left(a_{K,E}\psi_{w,K} - \sum_{F\in\mathcal{E}_K} a_{K,E,F}\psi_{w,F}\right), \qquad (30)$$

where $a_{K,E} = \sum_{F\in\mathcal{E}_K} a_{K,E,F}$. In (30) we assume that the side-average potentials $\psi_{w,E}$ are continuous across the internal sides, i.e., $\psi_{w,K_1,E} = \psi_{w,K_2,E} = \psi_{w,E}$, for all neighboring elements K_1 and K_2 of $E \in \mathcal{E}_h^{int}$. Additionally, we drop out the element index K from the side–average potential $\psi_{w,K,E} = \psi_{w,E}$ also for all external (boundary) sides $E \in \mathcal{E}_h^{ext}$.

Similarly, the expression of the capillary velocity $\mathbf{u}_c$ in the basis of $\mathbf{RT}_0(K)$ reads as

$$u_{c,K,E} = \lambda_{t,K}\left(a_{K,E}\psi_{c,K} - \sum_{F\in\mathcal{E}_K} a_{K,E,F}\psi_{c,K,F}\right), \qquad (31)$$

where $\psi_{c,K,F}$ denotes the potential ψ_c averaged over side F with respect to element K for all $F \in \mathcal{E}_K$. Due to the extended capillary pressure condition at a material interface placed at side $E \in \mathcal{E}_h^{int}$, the side-average capillary potential $\psi_{c,E}$ can be discontinuous when the barrier effect is simulated. This situation requires careful treatment and is described in the following section. We drop out the element index K from the side-average potential $\psi_{c,K,E} = \psi_{c,E}$ also for all external (boundary) sides $E \in \mathcal{E}_h^{ext}$.

4.2. System of Equations for Capillary Potentials

Let us consider two neighboring elements K_1 and K_2. Assuming that no mass is produced or lost on an internal side $E \in \mathcal{E}_{K_1} \cap \mathcal{E}_{K_2}$, we consider the following balance of the normal components of the phase velocities across E:

$$u_{\alpha,K_1,E} + u_{\alpha,K_2,E} = 0, \quad \alpha \in \{w, n\}. \qquad (32)$$

It follows from the expression (22) for the capillary velocity $\mathbf{u}_c$ that a balance equation similar to (32) holds also for the normal components of the capillary velocity $\mathbf{u}_c$, [13]. Therefore, we use (31) in order establish the following system of linear equations in terms of the side-average potentials $\psi_{c,K,E}$ for all $E \in \mathcal{E}_h^{int}$, $E \in \mathcal{E}_{K_1} \cap \mathcal{E}_{K_2}$:

$$\lambda_{t,K_1}a_{K_1,E}\psi_{c,K_1} - \lambda_{t,K_1}\sum_{F\in\mathcal{E}_{K_1}} a_{K_1,E,F}\psi_{c,K_1,F} + \\ +\lambda_{t,K_2}a_{K_2,E}\psi_{c,K_2} - \lambda_{t,K_2}\sum_{F\in\mathcal{E}_{K_2}} a_{K_2,E,F}\psi_{c,K_2,F} = 0. \qquad (33)$$

If the capillary potential is continuous across side $F \in \mathcal{E}_{K_1} \cap \mathcal{E}_{K_2}$, the side-average potentials $\psi_{c,K_1,F}$ and $\psi_{c,K_2,F}$ coincide and we denote their common value as $\psi_{c,F}$. In case of the barrier effect at side F, the capillary potential is discontinuous across F and by $\psi_{c,F}$ we denote the side–average capillary pressure potential that corresponds to the element with lower entry pressure. Altogether, the following side-average potentials $\psi_{c,K_1,E}$ and $\psi_{c,K_2,E}$ are used in the expression for the side-velocities in (33):

$$\psi_{c,K_1,E} = \begin{cases} p_{d,K_1} - (\rho_n - \rho_w)\int_E \mathbf{g}\cdot\mathbf{x}\ \mathrm{d}\mathbf{x}, \\ \qquad\qquad\qquad \text{if } p_{c,K_2,E} < p_{d,K_1}, \\ \psi_{c,E}, \qquad\qquad \text{otherwise,} \end{cases} \qquad (34a)$$

$$\psi_{c,K_2,E} = \begin{cases} p_{d,K_2} - (\rho_n - \rho_w)\int_E \mathbf{g}\cdot\mathbf{x}\ \mathrm{d}\mathbf{x}, \\ \qquad\qquad\qquad \text{if } p_{c,K_1,E} < p_{d,K_2}, \\ \psi_{c,E}, \qquad\qquad \text{otherwise.} \end{cases} \qquad (34b)$$

In (33), the cell–average capillary potential $\psi_{c,K}$ can be directly computed using (13) for a given cell–average value of the saturation $S_{w,K}$.

Together with the boundary conditions used to close the system of equations (34) for the unknown side-average potentials $\psi_{c,K,E}$, we obtain a sparse system of linear equations that can be written in a matrix form as

$$\mathbf{M}_c\mathbf{\Psi}_c = \mathbf{b}_c, \qquad (35)$$

where the square, symmetric, and positive definite matrix $\mathbf{M}_c$ and the vectors $\mathbf{\Psi_c}$ and $\mathbf{b_c}$ have dimensions $\#\mathcal{E}_h$, where $\#\mathcal{E}_h$ denotes the total number of sides in $\mathcal{E}_h$. The components of the vector $\mathbf{\Psi}_c$ are the side average potentials $\psi_{c,E}$ for all $E \in \mathcal{E}_h$.

4.3. Discretization of Volumetric Balance Equation

In order to express $u_{a,K,E}$ given by (30) in terms of the side–average variables $\psi_{w,E}$ and $\psi_{c,E}$, we derive an explicit formula for the cell-average of the wetting phase potential $\psi_{w,K}$. We integrate the volumetric balance equation (17) for the total velocity $\mathbf{u}_t$ over $K \in \mathcal{K}_h$ and use the divergence theorem to obtain

$$\sum_{F\in\partial K} \int_F (\mathbf{u}_a + f_n \mathbf{u}_c)\cdot\mathbf{n}_{K,F} = F_K, \tag{36}$$

where F_K is the integrated right–hand–side of (17) over K. Since we approximate the fluxes $\mathbf{u}_a$ and $\mathbf{u}_c$ in $\mathbf{RT}_0(K)$, the properties of the basis functions (24) allow to rewrite (36) as

$$\sum_{E\in\mathcal{E}_K} u_{a,K,E} + \sum_{E\in\mathcal{E}_K} f_{n,E}^{upw}\, u_{c,K,E} = F_K, \tag{37}$$

where $f_{n,E}^{upw}$ is the side–average value of f_n taken in the upstream direction with respect to $u_{c,K,E}$. Replacing the side fluxes $u_{a,K,E}$ in (37) by (30), we obtain

$$\begin{aligned} \lambda_{t,K}\, a_K\, \psi_{w,K} - \lambda_{t,K} \sum_{E\in\mathcal{E}_K} a_{K,E}\, \psi_{w,E} = \\ F_K - \sum_{E\in\mathcal{E}_K} f_{n,E}^{upw}\, u_{c,K,E}, \end{aligned} \tag{38}$$

where $a_K = \sum_{E\in\mathcal{E}_K} a_{K,E}$. Finally, we write $\psi_{w,K}$ as

$$\psi_{w,K} = \frac{F_K}{\lambda_{t,K}\, a_K} + \sum_{E\in\mathcal{E}_K} \frac{a_{K,E}}{a_K}\, \psi_{w,E} - \sum_{E\in\mathcal{E}_K} \frac{f_{n,E}^{upw}}{\lambda_{t,K}\, a_K}\, u_{c,K,E}, \tag{39}$$

which allows to express the side fluxes $u_{a,K,E}$ given by (30) in terms of the unknown $\psi_{w,F}$ only

$$\begin{aligned} u_{a,K,E} = \frac{a_{K,E}}{a_K}\left(F_K - \sum_{F\in\mathcal{E}_K} f_{n,F}^{upw}\, u_{c,K,F}\right) + \\ \lambda_{t,K} \sum_{F\in\mathcal{E}_K} \left(\frac{a_{K,E}a_{K,F}}{a_K} - a_{K,E,F}\right)\psi_{w,F}. \end{aligned} \tag{40}$$

4.4. System of Equations for Wetting-Phase Potentials

As in the previous section, we consider two neighboring elements K_1 and K_2. The continuity of the normal components of the phase velocities across internal sides allows us to establish equation

$$u_{a,K_1,E} + u_{a,K_2,E} = 0, \tag{41}$$

for all $E \in \mathcal{E}_h^{int}$, $E \in \mathcal{E}_{K_1} \cap \mathcal{E}_{K_2}$. We use (40) in order to express (41) in terms of the side-average potentials $\psi_{w,F}$. Together with the boundary conditions, (41) leads to a sparse system of linear equations for the unknowns $\psi_{w,F}$ that can be written in the matrix form as

$$\mathbf{M}_a \mathbf{\Psi}_w = \mathbf{b}_a, \tag{42}$$

where the square matrix $\mathbf{M}_a$ and the vectors $\mathbf{\Psi_w}$ and $\mathbf{b_a}$ have dimensions $\#\mathcal{E}_h$. Similar to the matrix $\mathbf{M}_c$, the matrix $\mathbf{M}_a$ is symmetric and positive definite.

4.5. Saturation Approximation

We discretize the saturation equation (23) using the discontinuous Galerkin (DG) method which is locally conservative and flexible for complex unstructured geometries. The DG method approximates the weak solution $S_w = S_w(t,\mathbf{x})$ of (23) in a functional space $D_1(\mathcal{K}_h)$ of discontinuous functions that are piecewise linear on $K \in \mathcal{K}_h$. Note that there is no continuity requirements across the internal sides of $\mathcal{K}_h$. By $\varphi_{K,E}$, we denote the piecewise linear basis functions of $D_1(\mathcal{K}_h)$ associated with the edges for all $K \in \mathcal{K}_h$ and $E \in \mathcal{E}_K$. We choose $\varphi_{K,E}$ such that for all $K \in \mathcal{K}_h$, $E, F \in \mathcal{E}_K$, and $d = 1, 2$

$$\frac{1}{|E|_{\text{d-1}}} \int_E \varphi_{K,F} = \delta_{EF}. \tag{43}$$

In order to obtain the variational formulation of the continuity equation on each element K, we multiply (23) by the basis functions $\varphi_{K,E} \in D_1(\mathcal{K}_h)$, $E \in \mathcal{E}_K$, integrate over K, and using the Green theorem:

$$\begin{aligned} \int_K \phi \frac{\partial S_w}{\partial t}\varphi_{K,E} + \int_{\partial K} f_w \varphi_{K,E}\mathbf{u}_a\cdot\mathbf{n}_{\partial K} - \\ \int_K f_w \mathbf{u}_a\cdot\nabla\varphi_{K,E} = \int_K F_w \varphi_{K,E}. \end{aligned} \tag{44}$$

We express the approximated solution as

$$S_w(t,\mathbf{x}) \approx \sum_{K\in\mathcal{K}_h} \sum_{E\in\mathcal{E}_K} S_{w,K,E}(t)\varphi_{K,E}(\mathbf{x}), \tag{45}$$

for all $\mathbf{x} \in \Omega$ and $t \in (0,T)$, where the basis coefficients $S_{w,K,E}$ are time-dependent.

Using the expression of $\mathbf{u}_a$ in the basis of $\mathbf{RT}_0(K)$ in (25), we approximate the second and the third integral in the left–hand–side of (44) as follows

$$\int_{\partial K} f_w \varphi_{K,E}\mathbf{u}_a\cdot\mathbf{n}_{\partial K} \approx \sum_{H,F\in\mathcal{E}_K} f_{w,F}^{upw} u_{a,K,H} I_{K,H,E,F}, \tag{46}$$

$$\int_K f_w \mathbf{u}_a\cdot\nabla\varphi_{K,E} \approx f_{w,K} \sum_{G\in\mathcal{E}_K} u_{a,K,G} J_{K,G,E}, \tag{47}$$

where $f_{w,K}$ is the cell-average of f_w, $f_{w,F}^{upw}$ is the side-average of f_w taken in the upstream direction with respect to $u_{a,K,F}$ and

$$I_{K,H,E,F} = \frac{1}{|H|_{\text{d-1}}} \int_H \varphi_{K,F}\varphi_{K,E}, \quad J_{K,G,E} = \delta_{EG} - \frac{1}{d+1}. \tag{48}$$

Using (45), the equation (44) reads as

$$\phi_K \sum_{F\in\mathcal{E}_K} \frac{\mathrm{d}S_{w,K,F}}{\mathrm{d}t} B_{K,E,F} + \sum_{H,F\in\mathcal{E}_K} f_{w,F}^{upw} u_{a,K,G} I_{K,H,E,F} - f_{w,K} \sum_{G\in\mathcal{E}_K} u_{a,K,G} J_{K,G,E} = F_{w,K,E}, \tag{49}$$

where ϕ_K denotes the cell-average value of the porosity ϕ. In (49), we introduce

$$B_{K,E,F} = \int_K \varphi_{K,E}\ \varphi_{K,F}, \quad F_{w,K,E} = \int_K F_w\ \varphi_{K,E}. \tag{50}$$

It follows from the properties (43) of the basis functions $\varphi_{K,E}$ that the coefficients $\mathbf{B}_K = \{B_{K,E,F}\}_{E,F\in\mathcal{E}_K}$ form a symmetric and positive definite matrix $\mathbf{B}_K$ and by $\mathbf{b}_K = \{b_{K,E,F}\}_{E,F\in\mathcal{E}_K}$, we denote its inversion, i.e., $\mathbf{b}_K = \mathbf{B}_K^{-1}$. Note that the matrix $\mathbf{B}_K$ is a $(d+1)\times(d+1)$ matrix and thus the computation of its inversion is cheap. Using the inverse matrix $\mathbf{B}_K^{-1} = \mathbf{b}_K$ in (49), the time derivatives of $S_{w,K,E}$ are explicitly given by the following ordinary differential equation (ODE)

$$\frac{\mathrm{d}S_{w,K,E}}{\mathrm{d}t} = \sum_{H\in\mathcal{E}_K} \frac{b_{K,E,H}}{\phi_K} \Bigg[F_{w,K,H} + \sum_{H,F\in\mathcal{E}_K} f_{w,F}^{upw} u_{a,K,G} I_{K,H,E,F} - f_{w,K} \sum_{G\in\mathcal{E}_K} u_{a,K,G} J_{K,G,E} \Bigg], \tag{51}$$

for all $K\in\mathcal{K}_h$ and $E\in\mathcal{E}_K$.

We use the explicit forward Euler method to solve the system of ODEs (51) where the initial condition is given by the initial condition for the saturation (15). Due to the higher–order approximation of the saturation in the discontinuous Galerkin method, the numerical scheme produces non-physical oscillations near shocks, [10], [13]. These spurious oscillations can be avoided by reconstructing the approximated discontinuous Galerkin solution using a slope limiter procedure. To stabilize the MHFE-DG numerical scheme, we use the slope limiter introduced by Chavent and Jaffré, [5], in the form described in [10].

4.6. Computational Algorithm

We summarize the complete computational algorithm for obtaining the numerical solution of the two-phase flow system (14) using the MHFE-DG method described in previous sections. The computation proceeds in the following order:

1. For a given mesh $\mathcal{K}_h$, compute the mesh-dependent coefficients $a_{K,E,F}$, $a_{K,E}$, and a_K for all $K\in\mathcal{K}_h$ and $E,F\in\mathcal{E}_K$.
2. Set $i=0$, $t=t_0$, and choose an initial time step Δt_0. Use (15) to initialize $S_{w,K,E}^0 = S_{w,K,E}^{ini}$.
3. Repeat the following steps until the predetermined final time T of the simulation is reached.
   (a) Based on a given saturations $S_{w,K,E}^i$ from previous time t_i, compute the cell-average capillary potentials $\psi_{c,K}$ for all $K\in\mathcal{K}_h$ using (13).
   (b) Assemble the matrix $\mathbf{M}_c$ and the vector $\mathbf{b}_c$ in (35).
   (c) Solve (35) and compute $u_{c,K,E}$ for $K\in\mathcal{K}_h$ and $E\in\mathcal{E}_K$ using (31).
   (d) Assemble the matrix $\mathbf{M}_a$ and the vector $\mathbf{b}_a$ given by (42).
   (e) Solve (42) and compute $u_{a,K,E}$ for $K\in\mathcal{K}_h$ and $E\in\mathcal{E}_K$ using (40).
   (f) Use the forward Euler method to obtain $S_{w,K,E}^{i+1}$ from (51).
   (g) Apply the slope limiting procedure in the form described in [10].
   (h) Set $t_{i+1} = t_i + \Delta t_i$ and set $i := i+1$.

In steps 3.c and 3.e, a direct or an iterative linear solver for sparse, symmetric, and positive definite matrices can be used.

5. Numerical Experiments

The correctness and accuracy of the MHFE-DG numerical scheme is verified by means of the semi-analytical solutions that can be obtained if several assumptions are placed upon the problem formulation (14). These benchmark solutions can be derived for a one-dimensional two-phase flow problem without sources or sinks ($F_w = F_n = 0$) and with zero gravity ($\mathbf{g} = 0$) for homogeneous and heterogeneous cases, see [2], [6], and [7]. In both benchmark problems we assume that the air ($\mu_n = 1.8205\cdot 10^{-5} kg\ m^{-1}s^{-1}$ and $\rho_n = 1.2\ kg\ m^{-1}s^{-1}$) displaces water ($\mu_w = 0.001\ kg\ m^{-1}s^{-1}$ and $\rho_w = 1000\ kg\ m^{-3}$) from a one-dimensional domain.

In order to test treatment of the barrier effect by our numerical scheme, we use the barrier effect test problem in layered porous medium described in [9]. As a benchmark solution, we used a numerical solution computed using the standard vertex-centered finite volume method (VCFVM) on a very fine mesh. The VCFVM numerical scheme used in this paper is described in [8].

5.1. Benchmark Solution in Homogeneous Medium

We test the numerical scheme by means of the McWhorter and Sunada problem formulation described in [6] in a one-dimensional domain $\Omega = [0,1]$ with the following choice of the parameters: $R = 0.92$, $S_0 = 0.5$, $S_i = 1$, and $A = 1.53\cdot 10^{-3}\ ms^{-\frac{1}{2}}$ (for the definition of these parameters, we refer to [6]). The properties of the porous medium are given in Table 2, Sand A.

$h_1 \to h_2$ [cm]	Homogeneous Case		Heterogeneous Case	
	eoc_1	eoc_2	eoc_1	eoc_2
$2 \to 1$	0.90	0.68	0.81	0.55
$1 \to 1/2$	0.77	0.49	0.87	0.62
$1/2 \to 1/4$	0.89	0.75	0.93	0.72
$1/4 \to 1/8$	0.87	0.89	0.91	0.63
$1/8 \to 1/16$	0.76	1.02	0.92	0.63

Table 1: Experimental orders of convergence eoc_1 and eoc_2 computed for the benchmark problems in homogeneous (left column) and heterogeneous (right column) porous medium in L_1 and L_2 norms, respectively.

In the MHFE-DG numerical scheme, we set $S_w^{ini} = S_i = 1$. At the inlet ($x = 0$), we prescribe the air and water Neumann boundary velocities to $u_n^{\mathcal{N}}(t,0) = At^{-\frac{1}{2}}$ and $u_w^{\mathcal{N}}(t,0) = (R-1)At^{-\frac{1}{2}}$, respectively. At the outlet ($x = 1\ m$), we set $u_w^{\mathcal{N}}(t,1) = RAt^{-\frac{1}{2}}$ and $S_w^{\mathcal{D}}(t,1) = S_i = 1$. We choose the final time $T = 1000\ s$ so that the air-front stays inside Ω. We compute the numerical solutions on a series of regular meshes with decreasing mesh sizes and compare them to the semi-analytical solution (see Figure 3a). The ratio $\Delta t/h^2$ is kept constant. We present the experimental orders of convergence (eoc) in Table 1 we show that the MHFE-DG method converge towards the exact solution.

5.2. Benchmark Solution in Heterogeneous Medium

We consider the Fučík *et al.* semi-analytical solution described in [7] for the two-phase flow in a porous medium with a single material discontinuity with the following choice of parameters: $R = 0.9$, $S_i^I = 0.3$, and $S_i^{II} = 1$ (for the definition of these parameters, we refer to [7]). The properties of the Sand A in $\Omega^I = [0, 1/2]$ and Sand B in $\Omega^{II} = [1/2, 1]$ are given in Table 2.

In the numerical model, we consider the following initial and boundary conditions. Initially, $S_w(0,x) = 0.3$ in Ω^I and $S_w(0,x) = 1$ in Ω^{II}. At $x = 0$, we set $S_w^{\mathcal{D}}(t,0) = 0.3$ and $\psi^{\mathcal{D}}(t,0) = 0\ Pa$. The boundary conditions at $x = 1$ read as $u_n^{\mathcal{N}}(t,1) = 0\ ms^{-1}$ and $u_w^{\mathcal{N}}(t,1) = RAt^{-\frac{1}{2}}$, where $A = 5.61 \cdot 10^{-4}\ ms^{-\frac{1}{2}}$. The numerical solution compared to the semi-analytical solution is shown in Figure 3b. The experimental orders of convergence (eoc) in Table 1 show that the MHFE-DG method converges towards the exact solution.

5.3. Barrier Effect Test Problem in Layered Porous Medium

In principle, the benchmark solution used in the previous section cannot simulate the barrier effect because it always requires a non-zero flux of the non-wetting phase across the material interface [7]. In order to verify simulation of the barrier effect using our numerical scheme, we use the problem formulation described in [9, page 275]. Here, a non-wetting phase ($\mu_n = 10^{-3}\ kg\ m^{-1}s^{-2}$ and $\rho_n = 1400\ kg\ m^{-3}$) displaces water from an initially fully water-saturated, vertically placed column shown in Figure 4a. The column consists of three sand layers with two different sands denoted as Sand C and Sand D (see Table 2). The sharp material interfaces are placed at $0.145\ m$ and $0.345\ m$, see Figure 4a. At the inlet boundary Γ_1, the DNAPL velocity is prescribed as $3.57 \cdot 10^{-5}\ ms^{-1}$ whereas the water velocity is zero. At the bottom of the column, the maximal wetting-phase saturation $S_w = 1$ is prescribed and the water pressure is kept constant at $2 \cdot 10^5\ Pa$. We use the following boundary conditions:

$$\mathbf{u}_n \cdot \mathbf{n} = -3.57 \cdot 10^{-5}\ ms^{-1} \quad \text{on } \Gamma_1 \tag{52a}$$
$$\mathbf{u}_w \cdot \mathbf{n} = 0 \quad \text{on } \Gamma_1, \tag{52b}$$
$$S_w = 1 \quad \text{on } \Gamma_3, \tag{52c}$$
$$\psi_w = 2 \cdot 10^5 + 4905\ Pa \quad \text{on } \Gamma_3, \tag{52d}$$
$$\mathbf{u}_n \cdot \mathbf{n} = 0 \quad \text{on } \Gamma_2 \cup \Gamma_4 \tag{52e}$$
$$\mathbf{u}_w \cdot \mathbf{n} = 0 \quad \text{on } \Gamma_2 \cup \Gamma_4, \tag{52f}$$

where $\mathbf{n}$ is the outer normal to the domain boundary. Initially, the column is fully water saturated, i.e., $S_w = 1$ in Ω. The initial mesh is shown in Figure 4b. The final time of the simulation $T = 1650\ s$ is chosen such that the DNAPL front stays inside the domain.

In Figure 5, we plot the numerical solutions obtained using the one-dimensional variant ($d = 1$) of the MHFE-DG method on vertical slice of the layered medium and compare them to the numerical solution obtained using the VCFVM method on a very fine mesh with mesh size $h = 1/256\ cm$. In order to show convergence of the numerical simulations computed in the full two-dimensional domain, the initial mesh in Figure 4b is refined uniformly. In Figure 6, we plot the numerical solution using the MHFE-DG method and, on a slice $x = 0.25$, we compare it to the numerical solution obtained using the VCFVM on a very fine mesh. The numerical results converge towards the VCFVM solution and show a very good agreement with the results published in [9, page 275]. Therefore, the barrier effect is captured correctly in both 1D and 2D cases.

6. Conclusion

We used the mixed-hybrid finite element (MHFE) method together with the discontinuous Galerkin (DG) approach to develop a higher–order numerical scheme capable of simulating flow of two immiscible and incompressible fluids in heterogeneous porous materials in one- and two-dimensional domains. We extended the approach described in [13] so that the barrier effect can be simulated. We used the previously developed benchmark solutions to investigate the convergence of the MHFE-DG numerical scheme towards the exact solution. In case of heterogeneous porous materials, we used an example problem from literature to show that the behavior of the non-wetting phase at material discontinuities is treated correctly and that the numerical scheme is capable of simulating the barrier effect.

Property	Sand A	Sand B	Sand C	Sand D
Porosity ϕ [−]	0.448	0.418	0.40	0.39
Intrinsic permeability K $[10^{-11}m^2]$	1.631	1.437	50.4	5.26
Residual saturation S_{wr} [−]	0.265	0.037	0.08	0.10
Brooks and Corey λ [−]	4.660	5.323	3.86	2.49
Brooks and Corey p_d $[Pa]$	3450.18	4041.72	370	1324

Table 2: Properties of sands used in the numerical simulations.

Acknowledgment

Partial support of the project "Mathematical Modelling of Multiphase Porous Media Flow" 201/08/P567 of the Czech Science Foundation (GA ČR) and the project "Numerical Methods for Multiphase Flow and Transport in Subsurface Environmental Applications" KONTAKT ME10009, Czech Ministry of Education, Youth and Sports is acknowledged.

References

[1] J. Bear and A. Verruijt. *Modeling Groundwater Flow and Pollution.* D. Reidel, Holland, Dordrecht, 1990.

[2] M. Beneš, R. Fučík, J. Mikyška, and T. H. Illangasekare. Analytical and Numerical Solution for One-Dimensional Two-Phase Flow in Homogeneous Porous Medium. *Journal of Porous Media*, 12(12):1139–1152, 2009.

[3] R. H. Brooks and A. T. Corey. Hydraulic Properties of Porous Media. *Hydrology Paper 3*, 27, 1964.

[4] N. T. Burdine. Relative Permeability Calculations from Pore-Size Distribution Data. *Trans. AIME*, 198:71–78, 1953.

[5] G. Chavent and J. Jaffré. *Mathematical Models and Finite Elements for Reservoir Simulation.* North-Holland: Amsterdam, 1986.

[6] R. Fučík, J. Mikyška, M. Beneš, and T. H. Illangasekare. An Improved Semi-Analytical Solution for Verification of Numerical Models of Two-Phase Flow in Porous Media. *Vadose Zone Journal*, 6(1):93–104, 2007.

[7] R. Fučík, J. Mikyška, M. Beneš, and T. H. Illangasekare. Semianalytical Solution for Two-Phase Flow in Porous Media with a Discontinuity. *Vadose Zone Journal*, 7(3):1001–1007, 2008.

[8] R. Fučík, J. Mikyška, T. Sakaki, M. Beneš, and T. H. Illangasekare. Significance of Dynamic Effect in Capillarity during Drainage Experiments in Layered Soils. *Vadose Zone Journal*, 9:697–708, 2010.

[9] R. Helmig. *Multiphase Flow and Transport Processes in the Subsurface : A Contribution to the Modeling of Hydrosystems.* Springer Verlag, Berlin, 1997.

[10] H. Hoteit, P. Ackerer, R. Mosé, J. Erhel, and B. Philippe. New Two-Dimensional Slope Limiters for Discontinuous Galerkin Methods on Arbitrary Meshes. *Int. J. Numer. Meth. Engng.*, (61):2566–2593, 2004.

[11] H. Hoteit and A. Firoozabadi. Multicomponent Fluid Flow by Discontinuous Galerkin and Mixed Methods in Unfractured and Fractured Media. *Water Resources Research*, 41, 2005.

[12] H. Hoteit and A. Firoozabadi. An Efficient Numerical Model for Incompressible Two-Phase Flow in Fractured Media. *Advances in Water Resources*, 31(6):891–905, 2008.

[13] H. Hoteit and A. Firoozabadi. Numerical Modeling of Two-Phase Flow in Heterogeneous Permeable Media with Different Capillarity Pressures. *Advances in Water Resources*, 31(1):56–73, 2008.

[14] J. Mikyška, M. Beneš, and T. H. Illangasekare. Numerical Investigation of Non-Aqueous Phase Liquid Behavior at Heterogeneous Sand Layers Using VODA Multiphase Flow Code. *Journal of Porous Media*, 12(7):685–694, 2009.

[15] D. Nayagum, G. Schäfer, and R. Mosé. Modelling Two-Phase Incompressible Flow in Porous Media Using Mixed Hybrid and Discontinuous Finite Elements. *Computational Geosciences*, 8(1):49–73, 2004.

[16] M. I. de Neef and J. Molenaar. Analysis of DNAPL Infiltration in a Medium with a Low-Permeable Lens. *Computational Geosciences*, 1:191–214, 1997.

[17] K. Pruess. Grid Orientation and Capillary Pressure Effects in the Simulation of Water Injection into Depleted Vapor Zones. *Geothermics*, 20(5-6):257–277, 1991.

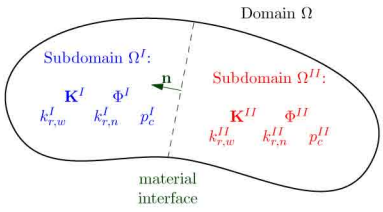

Figure 1: The sharp interface between two different porous media.

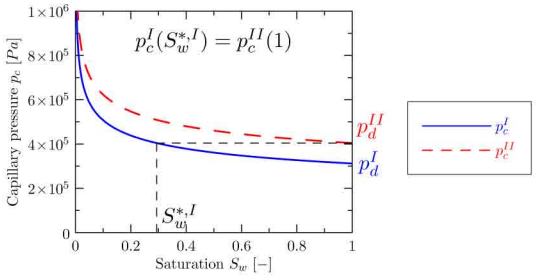

Figure 2: Typical Brooks and Corey capillary pressure curves for two different sands and the saturations at a material interface.

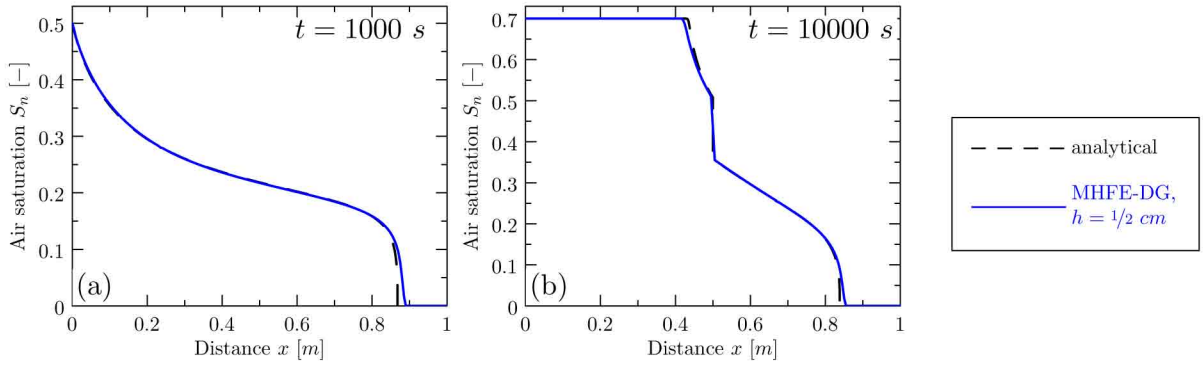

Figure 3: Numerical solution of the McWhorter and Sunada problem in a homogeneous (a) and heterogeneous (b) porous medium.

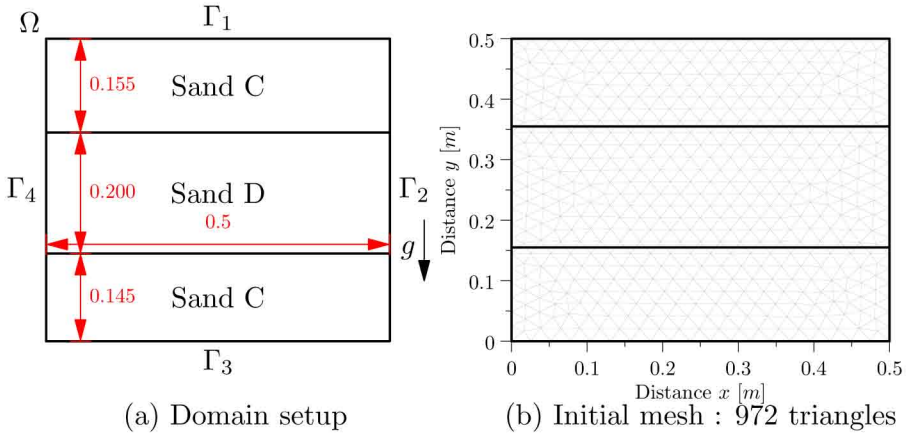

(a) Domain setup (b) Initial mesh : 972 triangles

Figure 4: Setup and the initial mesh for the barrier effect test problem.

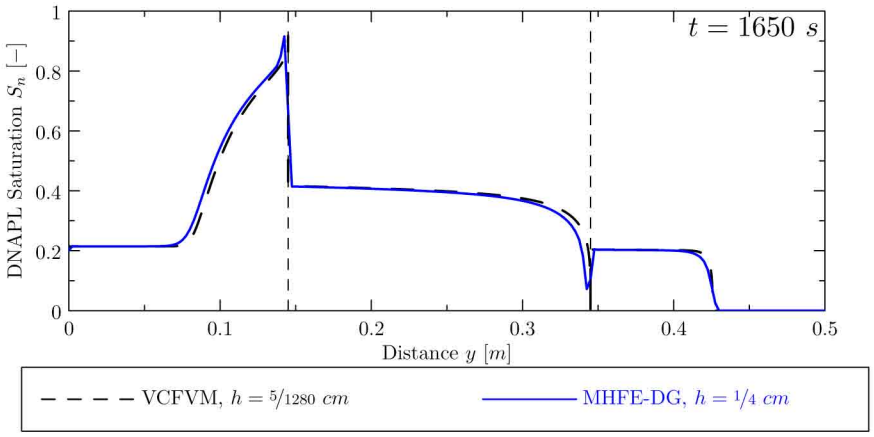

Figure 5: Comparison of the MHFE-DG method and the numerical solution obtained using the VCFVM on a very fine mesh for the barrier effect test problem. The time step Δt is chosen adaptively.

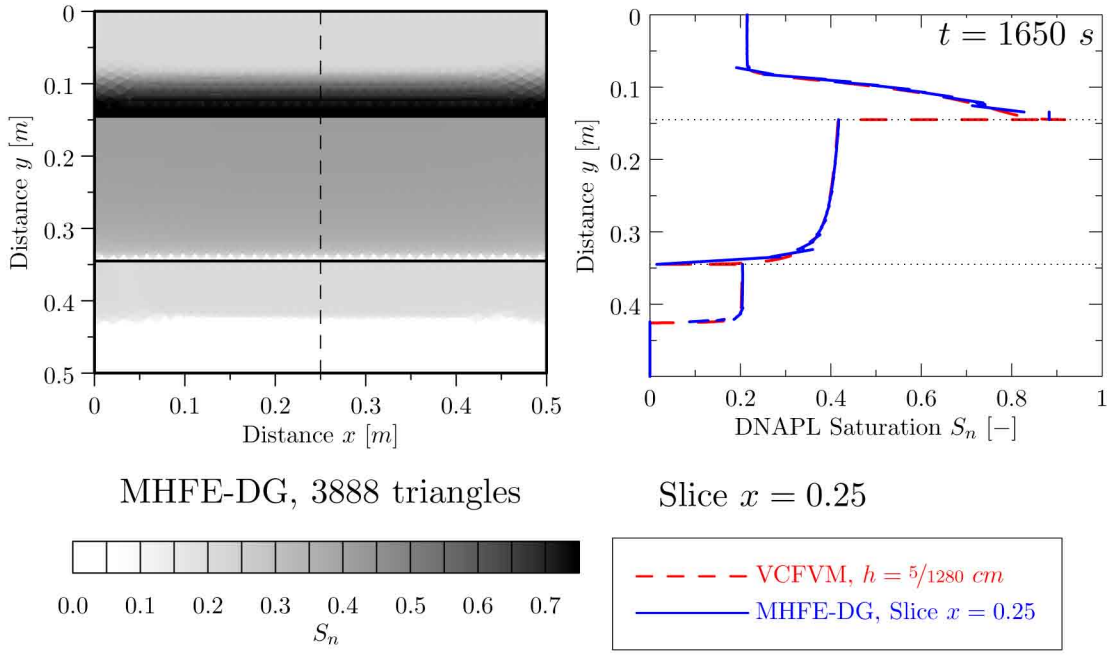

Figure 6: Numerical solutions of the barrier effect test problem using the MHFE-DG method in 2D. Slices of the numerical solution at $x = 0.25$ are compared to the numerical solution obtained using the VCFVM in 1D on a very fine mesh. The time step Δt is chosen adaptively.

Radek Fučík and Jiří Mikyška
Department of Mathematics, Faculty of Nuclear Sciences and Physical Engineering, Czech Technical University, Prague.
E-mail: radek.fucik(at)fjfi.cvut.cz
jiri.mikyska(at)fjfi.cvut.cz